## On-Demand Expansion Fluorescence and Photoacoustic Microscopy (ExFLPAM)

Xuan Mu<sup>1,†</sup>, Chenshuo Ma<sup>2,†</sup>, Xuan Mei<sup>1,†</sup>, Junlong Liao<sup>1</sup>, Rebecca Bojar<sup>1,3</sup>, Sizhe Kuang<sup>2</sup>, Qiangzhou Rong<sup>2</sup>, Junjie Yao<sup>2,\*</sup> and Yu Shrike Zhang<sup>1,\*</sup>

<sup>1</sup>Division of Engineering in Medicine, Department of Medicine, Brigham and Women's Hospital, Harvard Medical School, 65 Landsdowne Street, Cambridge, MA 02139, USA

<sup>&</sup>lt;sup>2</sup>Department of Biomedical Engineering, Duke University, Durham, NC 27708, USA

<sup>&</sup>lt;sup>3</sup>Barnard College, Columbia University, New York, NY 10027, USA

<sup>\*</sup>Corresponding authors. Emails: junjie.yao@duke.edu; yszhang@bwh.harvard.edu

<sup>†</sup>Equal Contribution

<sup>&</sup>lt;sup>#</sup>Current Address: Roy J Carver Department of Biomedical Engineering, College of Engineering, the University of Iowa, Iowa City, IA 52242, USA

**Abstract** 

Expansion microscopy (ExM) is a promising technology that enables nanoscale imaging on

conventional optical microscopes by physically magnifying the specimens. Here, we report the

development of a strategy that enables i) on-demand labeling of subcellular organelles in live cells

for ExM through transfection of fluorescent proteins that are well-retained during the expansion

procedure; and ii) non-fluorescent chromogenic color-development towards efficient bright-field

and photoacoustic imaging in both planar and volumetric formats, which is applicable to both

cultured cells and biological tissues. Compared to the conventional ExM methods, our strategy

provides an expanded toolkit, which we term as expansion fluorescence and photoacoustic

microscopy (ExFLPAM), by allowing on-demand fluorescent protein labeling of cultured cells, as

well as non-fluorescent absorption contrast-imaging of biological samples.

**Keywords** 

Expansion microscopy; Fluorescence imaging; Photoacoustic imaging; Transfection

2

#### Introduction

Expansion microscopy (ExM) has emerged as a promising technology for observing biological samples since it enables nanoscale imaging on conventional optical microscopes [1–4]. The key of ExM is the physical magnification of the specimens, where a swellable hydrogel plays an important role during this process [5–7]. In general, for ExM, target biomolecules and fluorescent tags are covalently anchored to the hydrogel network to maintain their relative positions in the hydrogel [8,9]. Specific proteolytic enzymes are introduced to break the cellular skeleton to avoid heterogeneous hydrogel swelling [10,11]. Finally, the hydrogel along with the specimen is expanded by immersing in a liquid of low osmolarity, which leads to an amplification of ~4.5× in linear dimension in a typical setup [2]. Up to now, various ExM methodologies have been developed for nanoscale imaging of proteins and nucleic acids within cells [12,13], which has already enabled successful high-resolution characterizations of samples that are both small, planar as well as large, three-dimensional, spanning across bacterial cells [14], mammalian cells [15], tissue sections [16], tissue blocks [17], and whole organisms [18].

Many efforts have been made to enhance the resolution limitation of ExM, such as using hydrogels with an increased swelling ability or repeating the expansion process [19–21], so far improved the magnification to ~20× [22]. To further enhance the ExM imaging, additional focus has been placed on the development of labeling strategies that ensure high labeling densities [23–25]. For such a perspective, genetically encoded fluorescent proteins through transfection might be a good alternative to antibodies. Similar to immunostaining, transfection methods can generate bright and photostable fluorescent signals, leading to convenient visualization of the labeled structures without the need for additional staining steps [26,27]. In addition, transfection methods may now be processed with ready-to-use reagents, eliminating complex protocols [28–31]. Nevertheless, on-demand transfection applied towards ExM usage has not been demonstrated yet.

Given the fact that fluorescent proteins have been shown to be directly expandable while maintaining their signals post-expansion [12,32], we therefore reasoned that transfection-enabled rapid labeling could potentially be applied to ExM as well. To confirm the hypothesis, we selected fluorescent proteins (green fluorescent protein, GFP and red fluorescent protein, RFP) to label subcellular organelles due to their resistance to proteinase-based digestion during the expansion process (Fig. 1) [33,34]. Since proteinase K is required for digestion to make samples mechanically homogenized, it is important to use proteinase-resistant proteins to preserve fluorescence signal.

With fluorescence microscope, the expanded samples were confirmed to show details in these labeled subcellular structures. In the meanwhile, to further broaden the suitability of the labeled specimens for a wide range of optical imaging modalities beyond fluorescence imaging, GFP and RFP were additionally immunolabelled with alkaline phosphatase (AP) and horseradish peroxidase (HRP), respectively. When subsequently incubated with Vector Blue and NovaRED, the enzyme substrates to AP and HRP, the structures produced corresponding blue and reddish-brown chromogen precipitants following the reactions. The chromogen precipitants, although nonfluorescent, have developed visual colors with strong optical absorption, which can then be imaged by photoacoustic microscopy (PAM) with favorable volumetric imaging ability and advanced imaging depth. Unlike traditional optical imaging techniques that have limited penetration in biological samples due to the strong light attenuation, PAM benefits from ultrasound detection of optical-absorption contrast [35]. This allows PAM to penetrate relatively deep within tissues for 3D imaging of biological specimens. Our methodology provides a new scheme to rapidly label subcellular organelles of interest for ExM, which also for the first time enables both fluorescence imaging and photoacoustic (PA) imaging with extended imaging capacities.

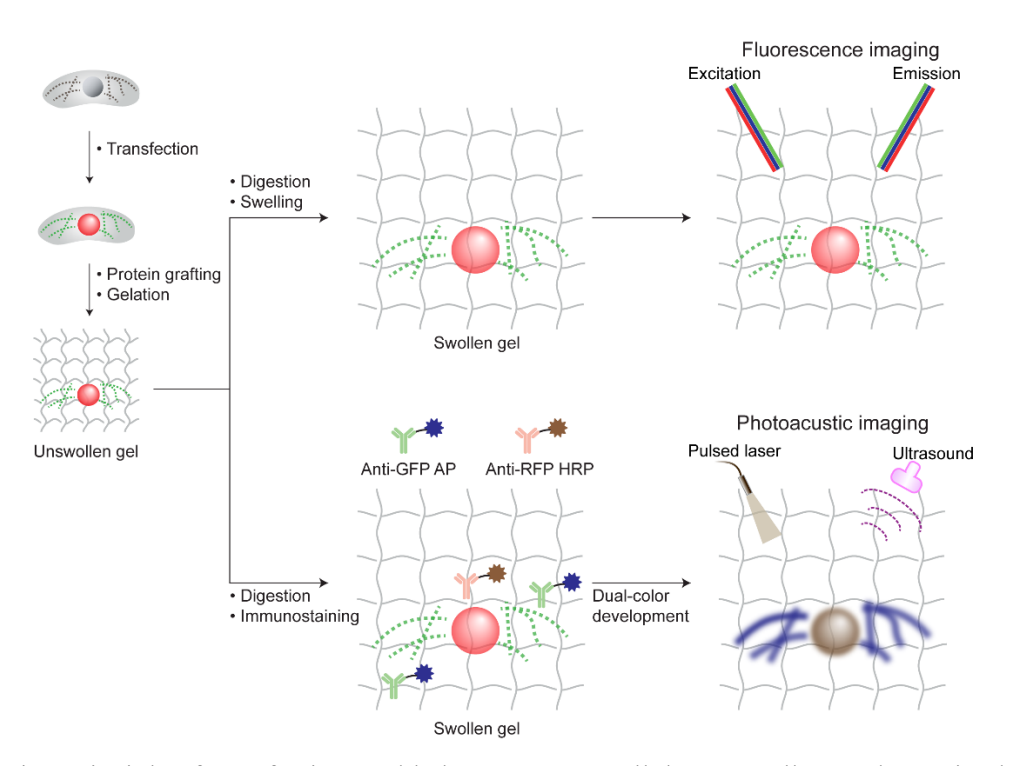


**Fig. 1.** Design principle of transfection-enabled ExFLPAM. Cellular organelles, such as mitochondria and nuclei, can be labeled by the transfection of fluorescent proteins (*e.g.*, GFP and RFP), followed by grafting

GFP and RFP onto the gel network. GFP and RFP are resistant to proteinase-based digestion. After digestion and swelling, the samples can be imaged under fluorescence microscope with improved spatial resolution. In addition, GFP and RFP can be further immunolabelled with enzymes such as AP and HRP. The swollen gel, after adding enzyme substrates, would develop visual colors, which may then be imaged by PAM with volumetric imaging capability and relatively large imaging depth.

#### **Results and Discussion**

The feasibility of the standard ExM protocol [2] was first confirmed on multiple cell types before the introduction of our intended transfection method. As shown in **Fig. S1a**, C2C12 myoblasts were immunostained with fluorescent antibody against tubulin and then processed with expansion. As anticipated, a ~4.3-fold linear expansion in tubulin diameter was achieved (**Fig. S1b**), which led to more sharply resolved microtubules than could be observed before expansion. Of note, the ExM technique has evolved into several variants with improved expansion ratios up to 20×, such as Magnify [9], ×10 microscopy [19], iterative ExM [20], and Ten-Fold Robust ExM [36]. However, most of these variants of ExM exhibit technical constraints compared to the original ExM, such as limited sample thickness, increased complexity of the procedure, uncommon reagents, or the compromised stability of expanding gels, which partially impede their adoption in the laboratory routine. Thus, we used the original protocol of ExM in the current work yet expect to incorporate the new variants in future works.

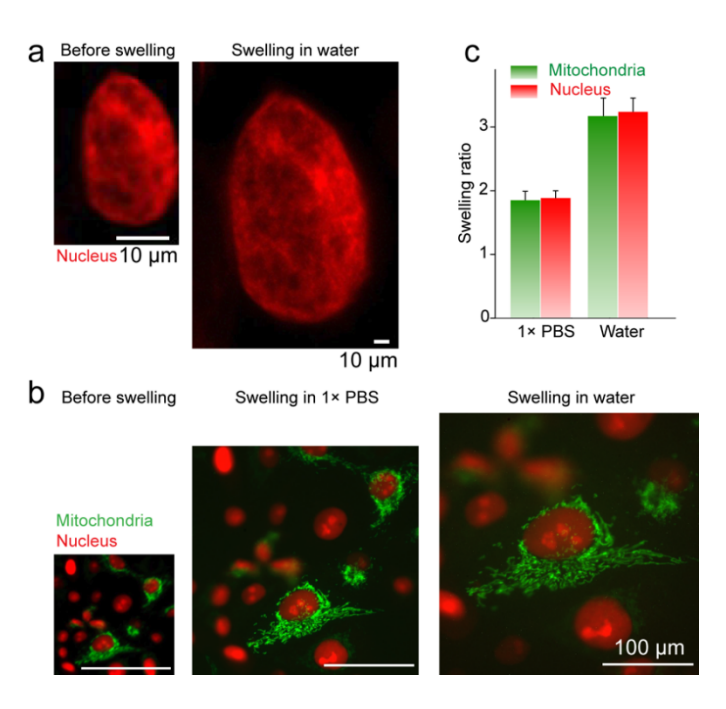


**Fig. 2.** On-demand transfection-enabled ExM. (a) Fluorescence imaging of the same RFP-labeled MCF-7 nucleus before and after swelling in water. (b) Fluorescence imaging of MCF-7 cells on-demand transfected for 24 h prior to ExM, showing GFP-labeled mitochondria and RFP-labeled nuclei in three different swelling statues after transfection (without swelling and swollen in 1× PBS and water). (c) Quantitative characterization of the swelling ratios of both organelles in 1× PBS and water, compared to that without swelling. N=3.

To subsequently confirm the compatibility of ExM with on-demand transfection-enabled labeling of subcellular organelles, wildtype cells without any intrinsic fluorescence emission were transfected with CellLight reagents for 24 h immediately prior to expansion, to explicitly express fluorescent proteins of desired colors on target structures. In one demonstration, the nuclei of MCF-7 cells were labeled with RFP. The transfection of foreign nucleic acids into cultured mammalian cells has a wide application in research for fluorescence labeling, gene-based therapy, and drug development, yet it may still be limited by cytotoxicity, cell-specific bias, and transfection ratio [37,38]. These restrictions would be minimal in our work, as ExM focuses on subcellular organelles. After treating the samples with the ExM protocol followed by swelling in 1× PBS and then water, the nuclei showed significantly improved detail in structures compared to non-expanded samples (Fig. 2a). As shown in Fig. 2b, in another dual-color demonstration, the mitochondria of MCF-7 cells were labeled with GFP while the nuclei were transfected to express RFP. With expansion, both mitochondria and nuclei were clearly expanded with substantially improved resolutions under fluorescence imaging. The expansion ratios of both organelles were quantified, resulting in ~1.7-fold in 1× PBS and ~3.1-fold in water, with no noticeable differences between the two labeled organelles (Fig. 2c) or with single labeling of the nuclei (Fig. 2a). Different from conventional immunostaining, transfection-induced fluorescent protein expression would be present and fused to the localization sequence within targeted intracellular structure before expansion. The fusion of proteinase-resistant fluorescent proteins (GFP and RFP) may protect these original proteins from digestion and result in insufficient mechanical homogenization. Thus, the expansion ratio reduced slightly compared to the original expansion protocol.

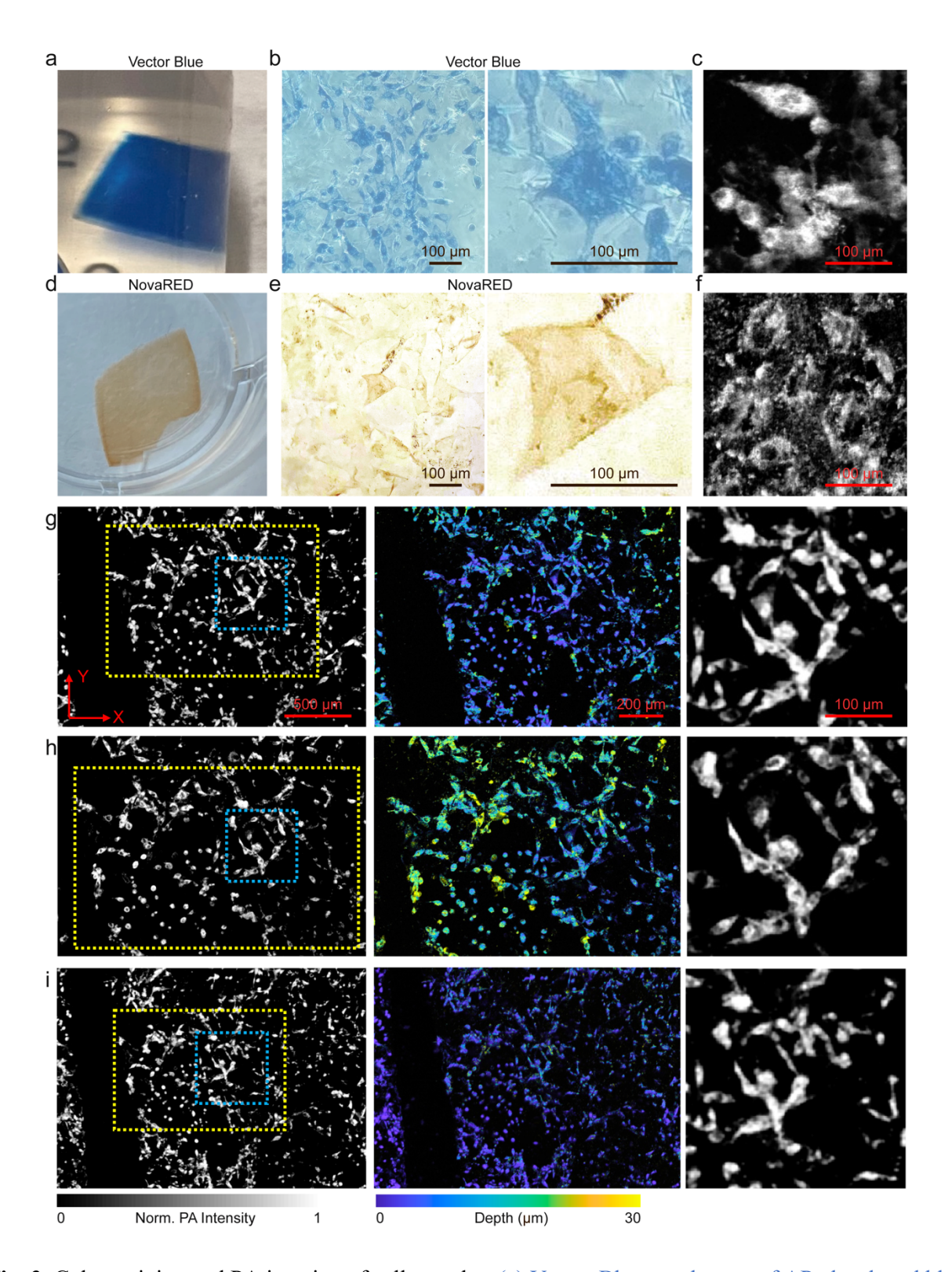


**Fig. 3.** Color staining and PA imaging of cell samples. (a) Vector Blue, a substrate of AP, developed blue color for AP-labeled cell samples. (b) Transmission-mode optical microscope images of blue stained HUVECs (transfected with GFP) in the gels. (c) TOR-PAM images of Vector Blue gel. (d) NovaRED, a

substrate of HRP, developed brown color for HRP-labeled cell samples. (e) Transmission-mode optical microscope images of brown-stained HUVECs (transfected with RFP) in the gels. (f) TOR-PAM images of HUVECs in the gel with NovaRED staining. (g-i) TOR-PAM images of Vector Blue gel (g) before, (h) after swelling in water, and (i) shrinking in 10× PBS. Yellow dotted squares indicate the same area of expansion and shrinking. Middle row: TOR-PAM depth-coded images. Right row: zoomed-in images of selected areas within blue dotted boxes.

While fluorescence imaging relies on the fluorescent emission of the transfected proteins, PAM does not. In fact, by detecting the optical absorption contrast, PAM can image both fluorescent and non-fluorescent molecules, which is much more flexible than traditional fluorescence imaging. In PAM, pulse-laser light is absorbed by biomolecules and the absorbed photon energy is converted into heat via the photothermal effect. The heat-induced expansion generates acoustic pressure waves that can be detected to map the original optical energy deposition in the sample. PAM is intrinsically a volumetric imaging modality, and takes advantage of the rich optical contrast of endogenous or exogenous biomolecules, as well as the deep-penetrating acoustic detection for superior imaging depth. We have previously demonstrated that PAM is able to perform multi-spectrum imaging of non-expanded biological samples stained with color-absorbing histology dyes [39]. In this study, we build a transmission optical-resolution photoacoustic microscopy (TOR-PAM) system (Fig. S2a) to achieve PA images with different color staining and a variety of depths. To this end, we rationed that, not only is it possible to retain the fluorescence signals post-expansion, but these fluorescent proteins may be further converted to optical absorption contrast for PAM, by applying, further, a color-developing protocol that is commonly used in conventional histology, which we term as ExFLPAM.

For TOR-PAM, the specimens must carry optical absorption contrasts for pulsed laser excitation and ultrasonic detection [40,41]. In an initial demonstration, a dual-absorbing-color staining strategy was developed by using chromogenic substrates for immunolabeled enzymes on fluorescent proteins. As examples, GFP-HUVECs were cultured, fixed, and immunolabeled with AP-anti-GFP; when they were expanded in 1× PBS and subsequently exposed to Vector Blue substrate specific for AP, strong blue-colored precipitations were produced leading to the entire gel turning blue visually (**Fig. 3a**). Similarly, when RFP-HUVECs were labeled with HRP-anti-RFP, expanded, and treated with NovaRED substrate specific to reaction with HRP, a strong brown-colored chromogenic contrast was developed (**Fig. 3d**). Since these are absorbing-only

contrasts, the cells were visible under bright-field microscopy without the need for fluorescence imaging, indicating blue and reddish-brown colors, respectively (Fig. 3b and 3e).

As previously discussed, the precipitations formed by these chromogens used for staining have strong optical absorptions across a wide wavelength range. Fig. S3 shows typical absorption spectra of precipitations formed from Vector Blue, NovaRED, and DAB substrates upon reaction with their corresponding specific enzymes. Accordingly, we developed a high-resolution TOR-PAM system with a spatial resolution of ~625 nm (Fig. S2b). It was clearly shown that the expanded cells stained with both Vector Blue (Fig. 3c) and NovaRED (Fig. 3f) could be imaged at 532 nm. The expansion ratio was also calculated on the Vector Blue-stained samples. Compared to cells before expanding (Fig. 3g), the gel expanded 1.32-fold to 1.37-fold after immersion in water (Fig. 3h). The expanded gel was further incubated in 10× PBS, where a shrinkage of 1.68fold to 1.78-fold was observed (Fig. 3i). The imaging of expanded and shrunken specimens was further confirmed with additional PA images (Fig. S4). Due to the use of 1× PBS during the labeling process, these samples were already slightly expanded prior to immersion in water. As compared to the transfected-only samples (Fig. 2), the expansion ratio was reduced from 1.82-fold to 1.37-fold after chromogenic labeling, which was possibly due to the formation of the precipitates on the hydrogel networks during the enzymatic reactions of chromogens that mechanically limited the full expansion of these gels. A similar observation was made when the expanded gel was shrunken back in 10× PBS. The NovaRED-stained cells exhibited similar expansion for PA imaging (Fig. S5). Notably, taking advantages of the acoustic penetration of PAM, volumetric cellular imaging was acquired from 0 µm (surface) to 30 µm in depth both before and after expansion (Fig. S6).

Finally, based on the above results, the mouse kidney tissues expressing GFP were further tested using the same absorbing color-enabled staining strategy. As revealed in **Fig. 4a and 4b**, the whole kidney slice could be successfully imaged by TOR-PAM at the wavelength of 532 nm, post-expansion in 1× PBS and post-staining with Vector Blue. Again, with the volumetric imaging ability of TOR-PAM, the expanded, stained tissue at different depths (0, 25 and 50 µm) was readily imaged (**Fig. 4c**). The selected areas in **Fig. 4c** showing detailed kidney structure such as convoluted proximal tubules (as indicated with arrows in **Fig. 4d**) otherwise not resolvable by PAM without expansion.

## **Conclusion**

In summary, we have developed a new strategy that enables *i*) on-demand labeling of subcellular organelles in live cells for ExM through transfection of fluorescent proteins that are well-retained during the expansion procedure; and *ii*) chromogenic color-development towards efficient bright-field and PAM imaging in both planar and volumetric formats, which is applicable to both cultured cells and biological tissues. These advances will likely further expand the applicability of ExM leading to additional capacities not possible or convenient before using immunostaining-based fluorescence imaging or fluorescent protein-labeled structures that does not allow absorbing contrasts.

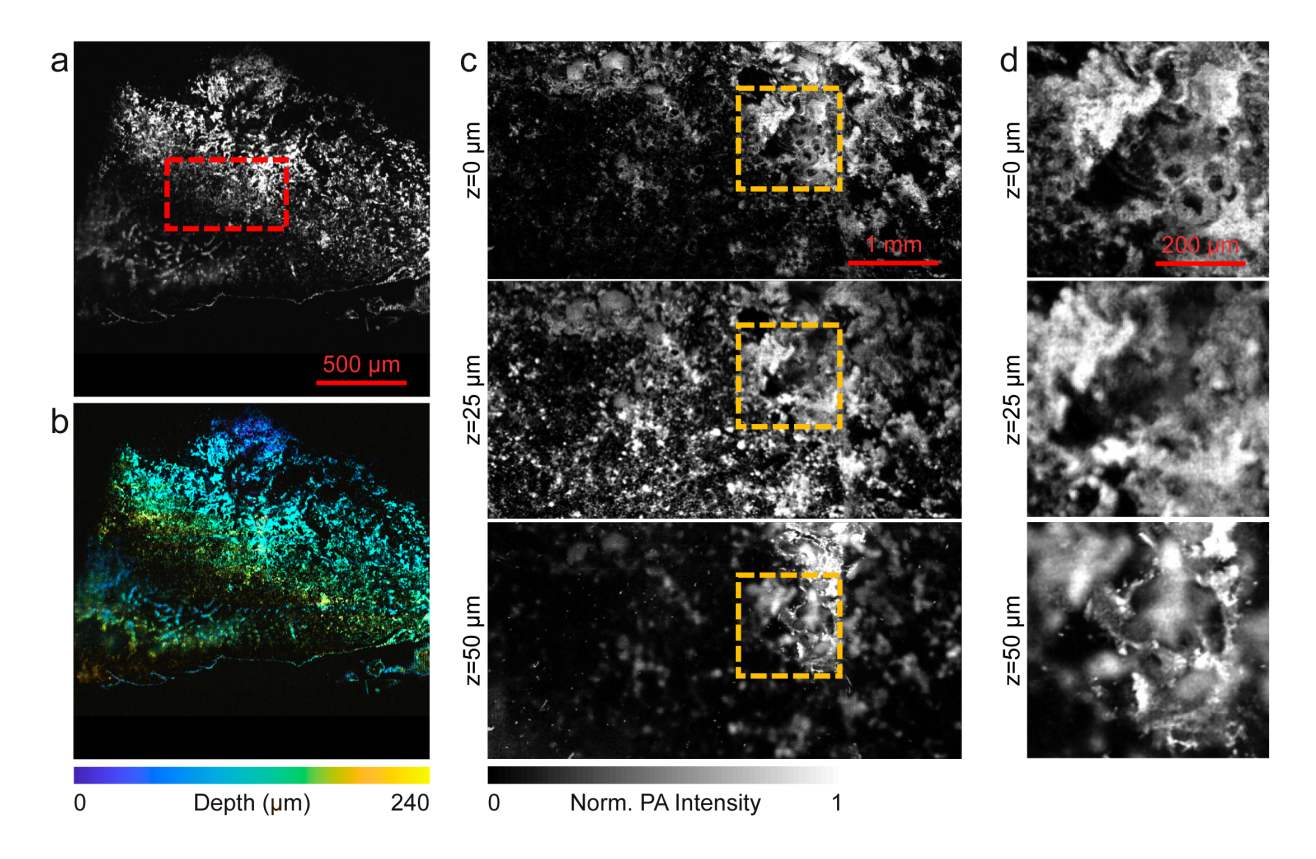


**Fig. 4.** TOR-PAM images of kidney slices. (a) Full-view image of the kidney sample. (b) TOR-PAM depth coding images of the same kidney sample as in (a). (c) Close-up images at different depths, as indicated by the red dashed box in (a). (d) Close-up images at different depths, as indicated by the yellow dashed boxes in (c).

We anticipate that the methodology delineated in this study will serve as the foundation for ExFLPAM, yet it necessitates further refinement to broaden its applicability. Nevertheless, our proof-of-concept studies do not come with no limitations and warrant further developments. First, ExFLPAM demonstrates commendable image quality for singularly stained cell and tissue samples using NovaRED or Vector Blue; however, the challenge persists when extending the technique to multi-color staining. PA imaging is a robust modality relying on distinct absorption wavelengths. Employing a multi-wavelength PA imaging platform should enhance our ability to discern intricate cell structures within multi-color staining samples. Second, the current TOR-PAM system exhibits a low imaging speed, limited by the slow mechanical scanning. To capture dynamic changes in live cells or organoids, it is necessary to improve the imaging speed of ExFLPAM. In addition, the promising directions of ExFLPAM also include the utility of platform microfluidic techniques [42] and cellular interactions in bacterial infection and wound healing [43–45].

Moreover, to simplify the conceptual demonstrations, we sticked to the very original yet most robust expansion protocol that only provides an expansion ratio of ~4-fold [2], which in certain cases such as transfection, was further reduced to ~3-fold possibly due to the insufficient mechanical homogenization after the enhanced expression of proteinase K resistant protein (GFP and RFP). The expansion ratio was also reduced after chromogenic labeling, which may be due to the confinement of the precipitates formed with the chromogen under enzymatic reactions, on the hydrogel network. Optimizations that would further improve the expansion ratio shall be investigated. in addition, compatibility of such a concept with other ExM variations, for example, iterative ExM [17,20], remains to be explored. Multi-spectral PAM imaging of multiple contrasts at the same time could be explored as well [46], given the broad availability of these chromogens that all have distinct absorption spectra across the wavelength range (e.g., Fig. 3e). In particular, the colors of the dye chromogens include red, magenta, purple, brown, blue, indigo, blue-gray, and gray-black, and have been used for triple-labeling of histological samples [47]. Nevertheless, several factors need to be considered for multispectral imaging, such as the compatibility of enzyme substrates. We anticipate that, with additional technical advancements based on our current concept, the strategy will find potential wide applicability in biology, bioimaging, biomedicine, and beyond.

## **Declaration of Competing Interest**

The authors declare that they have no known competing financial interests or personal relationships that could have appeared to influence the work reported in this paper.

## Acknowledgements

We acknowledge the support by the National Institutes of Health (R03EB122662, R01HL153857, R01HL166522, R01CA282451, UG3TR003274, UH3TR003274), the National Science Foundation (CBET-EBMS-1936105, CISE-IIS-2225698), the Chan Zuckerberg Initiative (2022-316709), and the Brigham research Institute (to Y.S.Z.), as well as R01EB028143, R01NS111039, and RF1NS115581 from the National Institutes of Health, CAREER award 2144788 from the National Science Foundation, and 226178 from the Chan Zuckerberg Initiative (to J.Y.).

#### References

- [1] G. Wen, V. Leen, T. Rohand, M. Sauer, J. Hofkens, Current progress in expansion microscopy: chemical strategies and applications, Chem. Rev. 123 (2023) 3299–3323. https://doi.org/10.1021/acs.chemrev.2c00711.
- [2] F. Chen, P.W. Tillberg, E.S. Boyden, Expansion microscopy, Science. 347 (2015) 543–548. https://doi.org/10.1126/science.1260088.
- [3] A.T. Wassie, Y. Zhao, E.S. Boyden, Expansion microscopy: principles and uses in biological research, Nat. Methods. 16 (2019) 33–41. <a href="https://doi.org/10.1038/s41592-018-0219-4">https://doi.org/10.1038/s41592-018-0219-4</a>.
- [4] A. Klimas, Y. Zhao, Expansion microscopy: toward nanoscale imaging of a diverse range of Biomolecules, ACS Nano. 14 (2020) 7689–7695. https://doi.org/10.1021/acsnano.0c04374.
- [5] R. Gao, C.-C. (Jay) Yu, L. Gao, K.D. Piatkevich, R.L. Neve, J.B. Munro, S. Upadhyayula, E.S. Boyden, A highly homogeneous polymer composed of tetrahedron-like monomers for high-isotropy expansion microscopy, Nat. Nanotechnol. 16 (2021) 698–707. <a href="https://doi.org/10.1038/s41565-021-00875-7">https://doi.org/10.1038/s41565-021-00875-7</a>.
- [6] S. Ghosh, B.S. Sapkota, R.S. Rao, S. Patil, C. Rajkumar, S. Lakshminarayan, Expansion microscopy: a revolution in diagnostic pathology, J. Microsc. 290 (2023) 3–9. https://doi.org/10.1111/jmi.13170.
- [7] M. Wang, W. Li, G. Tang, C.E. Garciamendez-Mijares, Y.S. Zhang, Engineering

- (bio)materials through shrinkage and expansion, Adv. Healthc. Mater. 10 (2021) 2100380. https://doi.org/10.1002/adhm.202100380.
- [8] R. Thielhorn, I. Heing-Becker, N. Hümpfer, J. Rentsch, R. Haag, K. Licha, H. Ewers, Controlled grafting expansion microscopy, Angew. Chem. Int. Ed. 62 (2023) e202302318. <a href="https://doi.org/10.1002/anie.202302318">https://doi.org/10.1002/anie.202302318</a>.
- [9] A. Klimas, B.R. Gallagher, P. Wijesekara, S. Fekir, E.F. DiBernardo, Z. Cheng, D.B. Stolz, F. Cambi, S.C. Watkins, S.L. Brody, A. Horani, A.L. Barth, C.I. Moore, X. Ren, Y. Zhao, Magnify is a universal molecular anchoring strategy for expansion microscopy, Nat. Biotechnol. 41 (2023) 858–869. https://doi.org/10.1038/s41587-022-01546-1.
- [10] S. Truckenbrodt, C. Sommer, S.O. Rizzoli, J.G. Danzl, A practical guide to optimization in X10 expansion microscopy, Nat. Protoc. 14 (2019) 832–863. https://doi.org/10.1038/s41596-018-0117-3.
- [11] C. Cvetkovic, M.C. Ferrall-Fairbanks, E. Ko, L. Grant, H. Kong, M.O. Platt, R. Bashir, Investigating the life expectancy and proteolytic degradation of engineered skeletal muscle biological machines, Sci. Rep. 7 (2017) 3775. https://doi.org/10.1038/s41598-017-03723-8.
- [12] F. Chen, A.T. Wassie, A.J. Cote, A. Sinha, S. Alon, S. Asano, E.R. Daugharthy, J.-B. Chang, A. Marblestone, G.M. Church, A. Raj, E.S. Boyden, Nanoscale imaging of RNA with expansion microscopy, Nat. Methods. 13 (2016) 679–684. https://doi.org/10.1038/nmeth.3899.
- [13] G. Wang, J.R. Moffitt, X. Zhuang, Multiplexed imaging of high-density libraries of RNAs with MERFISH and expansion microscopy, Sci. Rep. 8 (2018) 4847. https://doi.org/10.1038/s41598-018-22297-7.
- [14] R. Götz, T.C. Kunz, J. Fink, F. Solger, J. Schlegel, J. Seibel, V. Kozjak-Pavlovic, T. Rudel, M. Sauer, Nanoscale imaging of bacterial infections by sphingolipid expansion microscopy, Nat. Commun. 11 (2020) 6173. <a href="https://doi.org/10.1038/s41467-020-19897-1">https://doi.org/10.1038/s41467-020-19897-1</a>.
- [15] D. Gambarotto, F.U. Zwettler, M. Le Guennec, M. Schmidt-Cernohorska, D. Fortun, S. Borgers, J. Heine, J.-G. Schloetel, M. Reuss, M. Unser, E.S. Boyden, M. Sauer, V. Hamel, P. Guichard, Imaging cellular ultrastructures using expansion microscopy (U-ExM), Nat. Methods. 16 (2019) 71–74. https://doi.org/10.1038/s41592-018-0238-1.
- [16] T.J. Chozinski, C. Mao, A.R. Halpern, J.W. Pippin, S.J. Shankland, C.E. Alpers, B. Najafian, J.C. Vaughan, volumetric, nanoscale optical imaging of mouse and human kidney via

- expansion microscopy, Sci. Rep. 8 (2018) 10396. <a href="https://doi.org/10.1038/s41598-018-28694-2">https://doi.org/10.1038/s41598-018-28694-2</a>.
- [17] D. Sarkar, J. Kang, A.T. Wassie, M.E. Schroeder, Z. Peng, T.B. Tarr, A.-H. Tang, E.D. Niederst, J.Z. Young, H. Su, D. Park, P. Yin, L.-H. Tsai, T.A. Blanpied, E.S. Boyden, Revealing nanostructures in brain tissue via protein decrowding by iterative expansion microscopy, Nat. Biomed. Eng. 6 (2022) 1057–1073. <a href="https://doi.org/10.1038/s41551-022-00912-3">https://doi.org/10.1038/s41551-022-00912-3</a>.
- [18] L. Freifeld, I. Odstrcil, D. Förster, A. Ramirez, J.A. Gagnon, O. Randlett, E.K. Costa, S. Asano, O.T. Celiker, R. Gao, D.A. Martin-Alarcon, P. Reginato, C. Dick, L. Chen, D. Schoppik, F. Engert, H. Baier, E.S. Boyden, Expansion microscopy of zebrafish for neuroscience and developmental biology studies, PNAS. 114 (2017) E10799–E10808. <a href="https://doi.org/10.1073/pnas.1706281114">https://doi.org/10.1073/pnas.1706281114</a>.
- [19] S. Truckenbrodt, M. Maidorn, D. Crzan, H. Wildhagen, S. Kabatas, S.O. Rizzoli, X10 expansion microscopy enables 25-nm resolution on conventional microscopes, EMBO Rep. 19 (2018) e45836. <a href="https://doi.org/10.15252/embr.201845836">https://doi.org/10.15252/embr.201845836</a>.
- [20] J.-B. Chang, F. Chen, Y.-G. Yoon, E.E. Jung, H. Babcock, J.S. Kang, S. Asano, H.-J. Suk, N. Pak, P.W. Tillberg, A.T. Wassie, D. Cai, E.S. Boyden, Iterative expansion microscopy, Nat. Methods. 14 (2017) 593–599. <a href="https://doi.org/10.1038/nmeth.4261">https://doi.org/10.1038/nmeth.4261</a>.
- [21] O. M'Saad, J. Bewersdorf, Light microscopy of proteins in their ultrastructural context, Nat. Commun. 11 (2020) 3850. <a href="https://doi.org/10.1038/s41467-020-17523-8">https://doi.org/10.1038/s41467-020-17523-8</a>.
- [22] L.A. Campbell, K.E. Pannoni, N.A. Savory, D. Lal, S. Farris, Protein-retention expansion microscopy for visualizing subcellular organelles in fixed brain tissue, J. Neurosci. Methods. 361 (2021) 109285. https://doi.org/10.1016/j.jneumeth.2021.109285.
- [23] S.K. Saka, Y. Wang, J.Y. Kishi, A. Zhu, Y. Zeng, W. Xie, K. Kirli, C. Yapp, M. Cicconet, B.J. Beliveau, S.W. Lapan, S. Yin, M. Lin, E.S. Boyden, P.S. Kaeser, G. Pihan, G.M. Church, P. Yin, Immuno-SABER enables highly multiplexed and amplified protein imaging in tissues, Nat. Biotechnol. 37 (2019) 1080–1090. <a href="https://doi.org/10.1038/s41587-019-0207-y">https://doi.org/10.1038/s41587-019-0207-y</a>.
- [24] G. Wen, M. Vanheusden, V. Leen, T. Rohand, K. Vandereyken, T. Voet, J. Hofkens, A universal labeling strategy for nucleic acids in expansion microscopy, J. Am. Chem. Soc. 143 (2021) 13782–13789. <a href="https://doi.org/10.1021/jacs.1c05931">https://doi.org/10.1021/jacs.1c05931</a>.

- [25] R. Lin, Q. Feng, P. Li, P. Zhou, R. Wang, Z. Liu, Z. Wang, X. Qi, N. Tang, F. Shao, M. Luo, A hybridization-chain-reaction-based method for amplifying immunosignals, Nat. Methods. 15 (2018) 275–278. <a href="https://doi.org/10.1038/nmeth.4611">https://doi.org/10.1038/nmeth.4611</a>.
- [26] M. Zaccolo, F. De Giorgi, C.Y. Cho, L. Feng, T. Knapp, P.A. Negulescu, S.S. Taylor, R.Y. Tsien, T. Pozzan, A genetically encoded, fluorescent indicator for cyclic AMP in living cells, Nat. Cell Biol. 2 (2000) 25–29. <a href="https://doi.org/10.1038/71345">https://doi.org/10.1038/71345</a>.
- [27] A.Y. Ting, K.H. Kain, R.L. Klemke, R.Y. Tsien, Genetically encoded fluorescent reporters of protein tyrosine kinase activities in living cells, PNAS. 98 (2001) 15003–15008. https://doi.org/10.1073/pnas.211564598.
- [28] D.R. Tyson, S.P. Garbett, P.L. Frick, V. Quaranta, Fractional proliferation: a method to deconvolve cell population dynamics from single-cell data, Nat. Methods. 9 (2012) 923– 928. https://doi.org/10.1038/nmeth.2138.
- [29] F.M. Boyce, N.L. Bucher, Baculovirus-mediated gene transfer into mammalian cells., PNAS. 93 (1996) 2348–2352. <a href="https://doi.org/10.1073/pnas.93.6.2348">https://doi.org/10.1073/pnas.93.6.2348</a>.
- [30] D.M. Roth, I. Harper, C.W. Pouton, D.A. Jans, Modulation of nucleocytoplasmic trafficking by retention in cytoplasm or nucleus, J. Cell. Biochem. 107 (2009) 1160–1167. https://doi.org/10.1002/jcb.22218.
- [31] J. Dorney, F. Bonnier, A. Garcia, A. Casey, G. Chambers, H.J. Byrne, Identifying and localizing intracellular nanoparticles using Raman spectroscopy, Analyst. 137 (2012) 1111–1119. https://doi.org/10.1039/C2AN15977E.
- [32] P.W. Tillberg, F. Chen, K.D. Piatkevich, Y. Zhao, C.-C. (Jay) Yu, B.P. English, L. Gao, A. Martorell, H.-J. Suk, F. Yoshida, E.M. DeGennaro, D.H. Roossien, G. Gong, U. Seneviratne, S.R. Tannenbaum, R. Desimone, D. Cai, E.S. Boyden, Protein-retention expansion microscopy of cells and tissues labeled using standard fluorescent proteins and antibodies, Nat. Biotechnol. 34 (2016) 987–992. <a href="https://doi.org/10.1038/nbt.3625">https://doi.org/10.1038/nbt.3625</a>.
- [33] C.-F. Chiang, D.T. Okou, T.B. Griffin, C.R. Verret, M.N.V. Williams, Green fluorescent protein rendered susceptible to proteolysis: positions for protease-sensitive insertions, Arch. Biochem. Biophys. 394 (2001) 229–235. <a href="https://doi.org/10.1006/abbi.2001.2537">https://doi.org/10.1006/abbi.2001.2537</a>.
- [34] J. Neefjes, N.P. Dantuma, Fluorescent probes for proteolysis: tools for drug discovery, Nat. Rev. Drug Discov. 3 (2004) 58–69. <a href="https://doi.org/10.1038/nrd1282">https://doi.org/10.1038/nrd1282</a>.
- [35] H. Kim, J. Baik, S. Jeon, J. Kim, C. Kim, PAExM: label-free hyper-resolution photoacoustic

- expansion microscopy, Opt. Lett. 45 (2020) 6755–6758. <a href="https://doi-org.ezp-prod1.hul.harvard.edu/10.1364/OL.404041">https://doi-org.ezp-prod1.hul.harvard.edu/10.1364/OL.404041</a>.
- [36] H.G.J. Damstra, B. Mohar, M. Eddison, A. Akhmanova, L.C. Kapitein, P.W. Tillberg, Visualizing cellular and tissue ultrastructure using Ten-fold Robust Expansion Microscopy (TREx), Elife. 11 (2022) e73775. <a href="https://doi.org/10.7554/eLife.73775">https://doi.org/10.7554/eLife.73775</a>.
- [37] M. Zeitelhofer, J.P. Vessey, Y. Xie, F. Tübing, S. Thomas, M. Kiebler, R. Dahm, Highefficiency transfection of mammalian neurons via nucleofection, Nat. Protoc. 2 (2007) 1692–1704. https://doi.org/10.1038/nprot.2007.226.
- [38] O. Gresch, L. Altrogge, Transfection of difficult-to-transfect primary mammalian cells. in: J.L. Hartley (Ed.) Protein expression in mammalian cells: Methods and Protocols, Humana Press, Totowa, NJ, 2012: 65–74. <a href="https://doi.org/10.1007/978-1-61779-352-3">https://doi.org/10.1007/978-1-61779-352-3</a> 5.
- [39] Y.S. Zhang, J. Yao, C. Zhang, L. Li, L.V. Wang, Y. Xia, Optical-resolution photoacoustic microscopy for volumetric and spectral analysis of histological and immunochemical samples, Angew. Chem. Int. Ed. 53 (2014) 8099–8103. <a href="https://doi.org/10.1002/anie.201403812">https://doi.org/10.1002/anie.201403812</a>.
- [40] M. Xu, L.V. Wang, Photoacoustic imaging in biomedicine, Rev. Sci. Instrum. 77 (2006) 41101. https://doi.org/10.1063/1.2195024.
- [41] H.F. Zhang, K. Maslov, G. Stoica, L.V. Wang, Functional photoacoustic microscopy for high-resolution and noninvasive in vivo imaging, Nat. Biotechnol. 24 (2006) 848–851. https://doi.org/10.1038/nbt1220.
- [42] D. Zhang, W. Li, Y. Shang, L. Shang, Programmable microfluidic manipulations for biomedical applications, Eng. Regen. 3 (2022) 258–261. https://doi.org/10.1016/j.engreg.2022.06.001.
- [43] X. Lin, L. Cai, X. Cao, Y. Zhao, Stimuli-responsive silk fibroin for on-demand drug delivery, Smart Med. 2 (2023) e20220019. https://doi.org/10.1002/SMMD.20220019.
- [44] X. Cao, L. Sun, Z. Luo, X. Lin, Y. Zhao, Aquaculture derived hybrid skin patches for wound healing, Eng. Regen. 4 (2023) 28–35. <a href="https://doi.org/10.1016/j.engreg.2022.11.002">https://doi.org/10.1016/j.engreg.2022.11.002</a>.
- [45] Y. Gao, Q. Ma, Bacterial infection microenvironment-responsive porous microspheres by microfluidics for promoting anti-infective therapy, Smart Med. 1 (2022) e20220012. https://doi.org/10.1002/SMMD.20220012.
- [46] M. Li, Y. Tang, J. Yao, Photoacoustic tomography of blood oxygenation: a mini review,

Photoacoustics. 10 (2018) 65–73. https://doi.org/10.1016/j.pacs.2018.05.001.

[47] IHC Multiplexing-Learn multicolor IHC staining, 2022. https://vectorlabs.com/. (Accessed Nov 19 2023).

## **Supplementary Information**

# On-Demand Expansion Fluorescence and Photoacoustic Microscopy (ExFLPAM)

Xuan Mu<sup>1,†</sup>, Chenshuo Ma<sup>2,†</sup>, Xuan Mei<sup>1,†</sup>, Junlong Liao<sup>1</sup>, Rebecca Bojar<sup>1,3</sup>, Sizhe Kuang<sup>2</sup>, Qiangzhou Rong<sup>2</sup>, Junjie Yao<sup>2,\*</sup> and Yu Shrike Zhang<sup>1,\*</sup>

<sup>1</sup>Division of Engineering in Medicine, Department of Medicine, Brigham and Women's Hospital, Harvard Medical School, 65 Landsdowne Street, Cambridge, MA 02139, USA

<sup>&</sup>lt;sup>2</sup>Department of Biomedical Engineering, Duke University, Durham, NC 27708, USA

<sup>&</sup>lt;sup>3</sup>Barnard College, Columbia University, New York, NY 10027, USA

<sup>\*</sup>Corresponding authors. Emails: <u>junjie.yao@duke.edu</u>; <u>yszhang@bwh.harvard.edu</u>

<sup>†</sup>Equal Contribution

<sup>&</sup>lt;sup>#</sup>Current Address: Roy J Carver Department of Biomedical Engineering, College of Engineering, the University of Iowa, Iowa City, IA 52242, USA

#### Methods

#### Cell culture

For MCF-7 cells, the following cell medium was used: Dulbecco's modified Eagle medium (DMEM; 21063029, Gibco), supplemented with 10% fetal bovine serum (FBS; 10438026, Gibco), and 1% mL L<sup>-1</sup> penicillin-streptomycin (15140122, Gibco). For GFP-prelabeled or RFP-prelabeled HUVECs, Endothelial Cell Medium (1001, ScienceCell) was used. The cells were cultured at 37 °C with 5% CO<sub>2</sub>. The cells were detached from flasks using 0.05% trypsinethylenediaminetetraacetic acid (EDTA) (25300054, Gibco), centrifugated and diluted to 50,000 cells mL<sup>-1</sup>. For 24-well plate, a coverslip (13 mm in diameter) was inserted into each well and 1 mL of diluted cell suspension was added. The cells were cultured for 24 h before further use.

## **Cell fixation**

For cell fixation, cytoskeleton extraction buffer was prepared, which included Triton X-100 (X100, Sigma, 5% (w/v), 4 mL), 4-piperazinediethanesulfonic acid (PIPES; P6575, Sigma-Aldrich 1 M, Ph adjusted to 7.0 with 5-M sodium hydroxide solution, 4 mL), ethylene glycol-bis(2-aminoethylether)-N,N,N,N-tetraacetic acid (EGTA; 03777, Sigma-Aldrich, 10 mM, 4 mL), magnesium chloride (AM9530G, Invitrogen, 40 μL), and water (27.96 mL). For microtubule fixation, a fixation solution was prepared as following: 16% (w/v) paraformaldehyde (158127, Sigma-Aldrich, 1.5 mL), 8% (w/v) glutaraldehyde (G6257, Sigma-Aldrich, 0.1 mL), PBS 10× (0.8 mL), and water (5.6 mL). A reduction solution was prepared by dissolving sodium borohydride (452882, Sigma-Aldrich, 10 mg) in PBS (10 mL). A quenching solution was prepared by using glycine (G7126, Sigma-Aldrich, 375 mg), PBS 10× (5 mL), and water (45 mL).

For each well, cell culture medium was replaced by 500 mL of cytoskeleton extraction buffer and incubated 1 min at room temperature. Then the cytoskeleton extraction buffer was aspirated and 1 mL of microtubule fixation solution was added. After incubating for 10 min at room temperature, cells were treated with reduction solution for 7 min and with quenching solution for 10 min, separately.

## **Immunostaining**

To perform immunostaining, the samples were treated with 300 μL of MAXblock (15252, Active Motif) blocking medium for 2 h, followed by washing with 1 mL of MAXwash washing medium

(15254, Active Motif) for 10 min. The cells were incubated with the primary antibodies for 2 h at room temperature and another 2 h with secondary antibodies in the dark. The following primary antibodies were used: sheep polyclonal anti-tubulin (ATN02, Cytoskeleton, 1:500) and rabbit polyclonal anti-tubulin (AB6046, Abcam, 1:100). The secondary antibodies used were listed as below: goat anti-rabbit Alex 564 (A11035, Invitrogen, 1:100), donkey anti-sheep Alex 546 (A21098, Invitrogen, 1:100), rabbit anti-sheep HRP-conjugated (AB6747, Abcam, 1:500), anti-GFP (GOAT) antibody ALP-conjugated (600-105-215, Rockland Immunochemicals, 1:200) and anti-RFP (RABBIT) antibody HRP-conjugated (600-403-379, Rockland Immunochemicals, 1:200).

## **Transfection**

For cell transfection, the following CellLight<sup>TM</sup> reagents were used. CellLight<sup>TM</sup> Mitochondria-GFP (C10600, Invitrogen) and CellLight<sup>TM</sup> Nucleus-RFP (C10603, Invitrogen). According to manufacturer's instruction, cells were incubated with transfection reagents for 24 h before imaging.

## Gelation and digestion

To prepare the AcX stock solution, 5 mg of acryloyl-X (A20770, Invitrogen) and 500 μL of anhydrous DMSO (D12345, Invitrogen) were mixed. The stock solution was diluted in PBS (1:100) before use. To prepare the gelation solution, stock X (98%), TEMED (T7024, Sigma, 1%), and APS (248614, Sigma, 1%) were mixed on ice before use. The stock X was composed as following: sodium acrylate (408220, Sigma-Aldrich, 3.8 g per 10 mL), 0.5 mL of acrylamide (A9099, Sigma-Aldrich, 0.5 g mL<sup>-1</sup>), 0.75 mL of N,N-methylenebisacrylamide (146072, Sigma-Aldrich, 0.02 g Ml<sup>-1</sup>), 4 mL of sodium chloride (5 M, Sigma-Aldrich, 14.61 g per 50 mL), 1 mL of PBS 10×, and 1.3 mL of water.

The AcX solution was diluted in PBS (1:100 dilution) and added to cells for incubating overnight. After washing with PBS for 5 min on ice, 300 mL of gelation solution was added to each well and incubated for 5 min on ice. A customized gelation chamber was made according to previous study [1]. The cell culture coverslips were inverted and contacted with 40 mL of gelation solution in the gelation chamber. After incubated at 37 °C for 1 h, the gelation solution was. The cell culture coverslips with gel were collected from the chamber and transferred to glass slides. Strong digestion was performed by using strong digestion solution mixed with 99% digestion

buffer and 1% proteinase K (P8107S, NE Biolabs). Strong digestion solution was prepared as follow: 10 mL of Triton X-100 (T8787, Sigma-Aldrich, 5 w/v%), 0.2 mL of EDTA (15575020, Invitrogen), 5 mL of tris(hydroxymethyl)aminomethane (Tris; AM9856, Invitrogen), 20 mL of sodium chloride (S6546, Sigma-Aldrich). For digestion, samples were kept on a shaker with digestion solution at room temperature overnight in the dark.

## Color development through chromogenic staining

As described before, GFP-HUVECs were cultured, fixed, immunolabeled with AP-anti-GFP (600-105-215, Rockland Immunochemicals, 1:200) and expanded in 1× PBS. For color development, samples were then exposed to Vector Blue substrate specific for AP (SK-5300, Vector Laboratories). To prepare the substrate working solution, Vector Blue Reagent 1 (80 mL), Vector Blue Reagent 2 (80 mL) and Vector Blue Reagent 3 (45 mL) were added to Tris-HCl buffer (AM9855G, Invitrogen, 5 mL, pH=8.2-8.5). The samples were incubated with the substrate working solution for 30 min to develop the color and washed with 1× PBS for 5 min before imaging.

RFP-HUVECs were treated following the same protocol but immunolabeled with HRP-anti-RFP (600-403-379, Rockland Immunochemicals, 1:200). NovaRED kit (SK-4805, Vector Laboratories) was further used for color development. A substrate working solution was prepared according to the manufacturer's instruction. Briefly, NovaRED Reagent 1 (80 mL), NovaRED Reagent 2 (50 mL), NovaRED Reagent 3 (50 mL) and NovaRED Reagent 4 (80 mL) were added to NovaRed Diluent (5 mL). The samples were incubated with the substrate working solution for 15 min at room temperature and washed with 1× PBS for 5 min.

#### **Expansion**

After digestion, the detached gel was carefully collected. 10 mL of water was added to the sample and incubated at room temperature for 10 min for expansion. The expansion process was repeated 3 times. In other cases, PBS of different concentrations were also used for expansion.

#### **TOR-PAM**

TOR-PAM employs a tightly focused laser beam that is diffraction-limited, with the lateral resolution being primarily determined by the optical focal spot size. A laser (VPFL-G-20, Spectral Physics) was operated at 532 nm to provide the excitation light. The laser beam was focused by

an objective lens (Mitutoyo 50x M Plan APO) with an NA of 0.55, and delivered to the sample surface with a pulse energy of 800 nJ at 532 nm. On the other side of the sample, an ultrasonic transducer with a central frequency of 30 MHz (V214-BB-RM, Olympus-NDT) was used to detect the resultant PA signals. The sample was excited with LED light from the top, which after passing through the sample, was reflected in another direction by a dichroic mirror. An image was captured by a CCD camera.

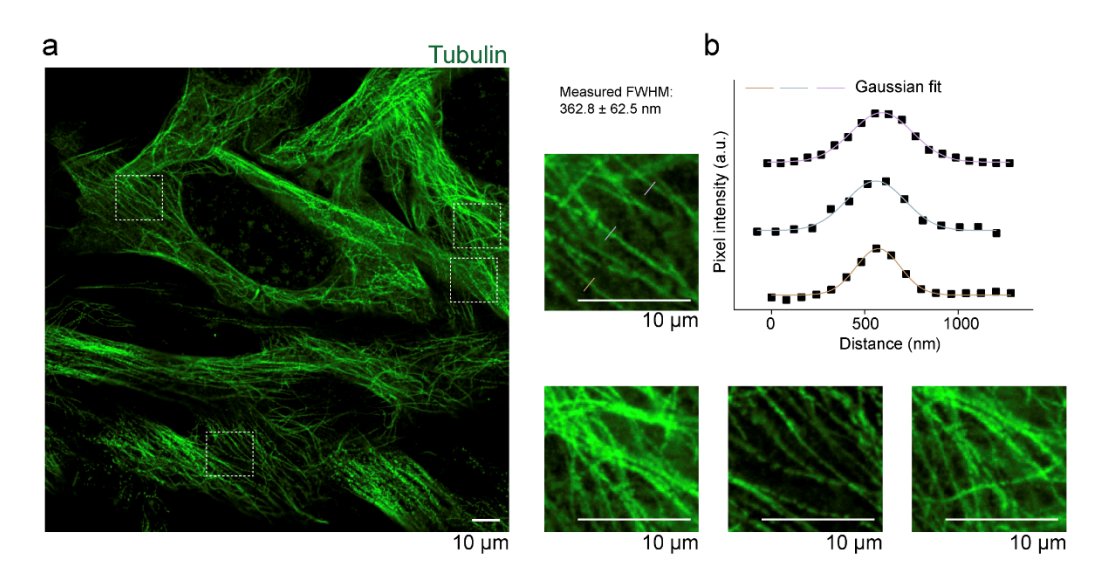


**Fig. S1.** Expansion characterization. (a) Typical ExM results of C2C12 tubulin expansion. (b) Quantification of the line width of single tubulin filaments after expansion.

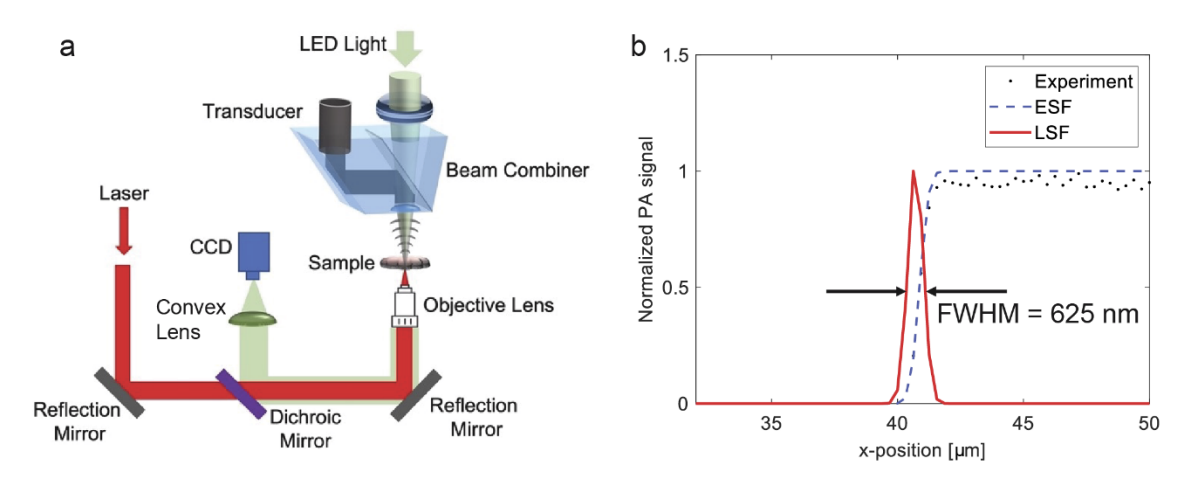


Fig. S2. (a) Schematic of TOR-PAM; (b) Lateral resolution measurement of TOR-PAM.

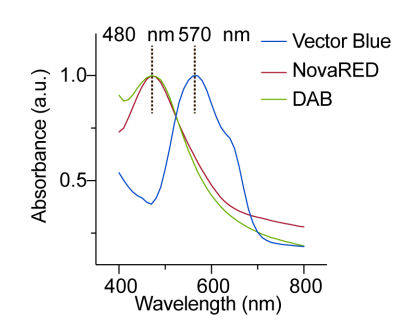
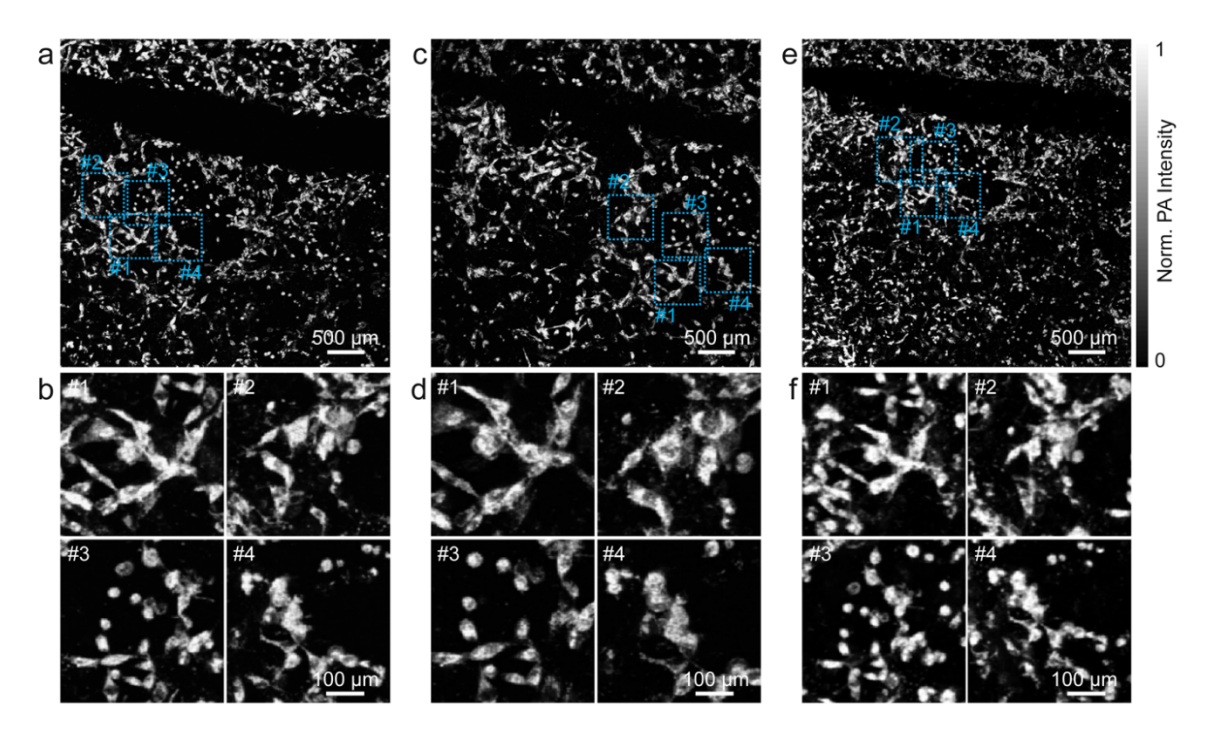
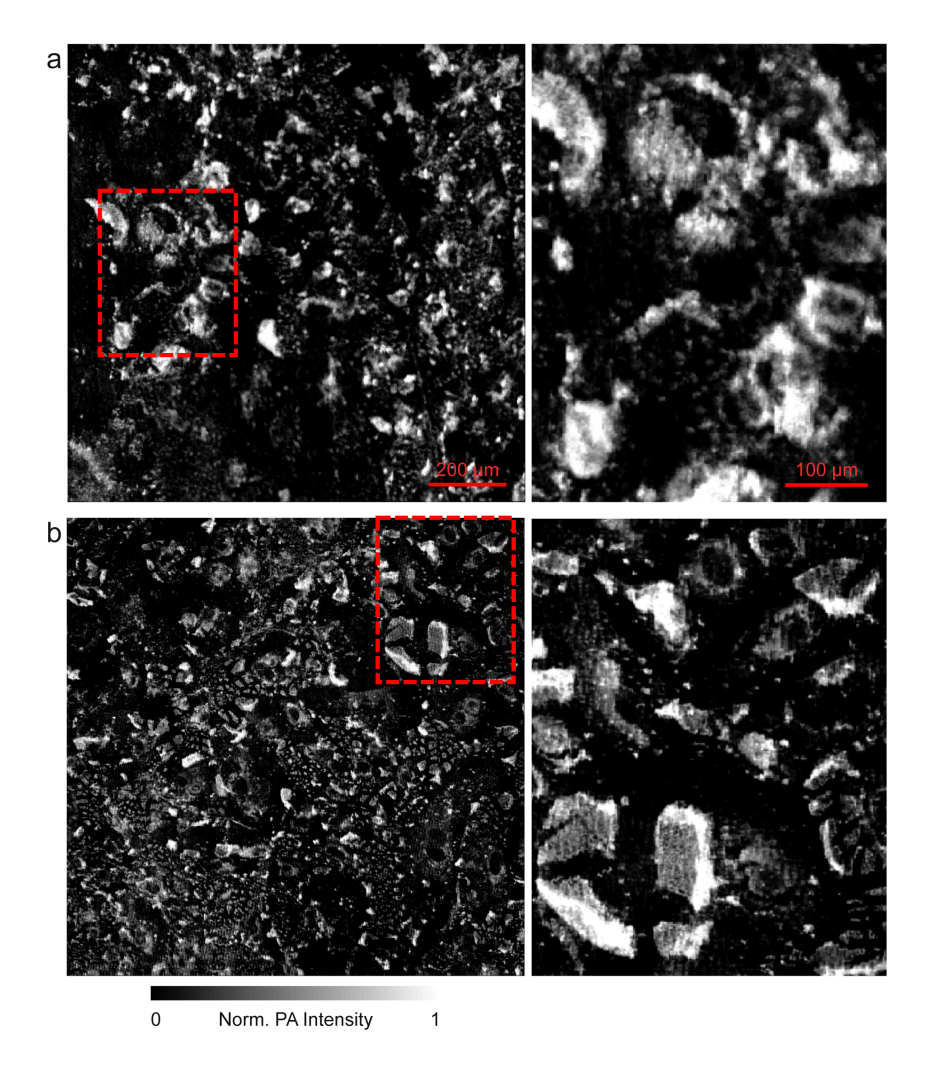


Fig. S3. Absorbance spectra of the stained colors by Vector Blue, NovaRED, and DAB.



**Fig. S4.** TOR-PAM images of Vector Blue-stained samples. (a) Gel before swelling. (c) Gel after swelling in water. (e) Gel shrinking back in 10× PBS. (b), (d), and (f) show magnified areas #1, #2, #3, and #4.



**Fig. S5.** TOR-PAM images of the swollen NovaRED-stained sample. (a) and (b) show two different areas.

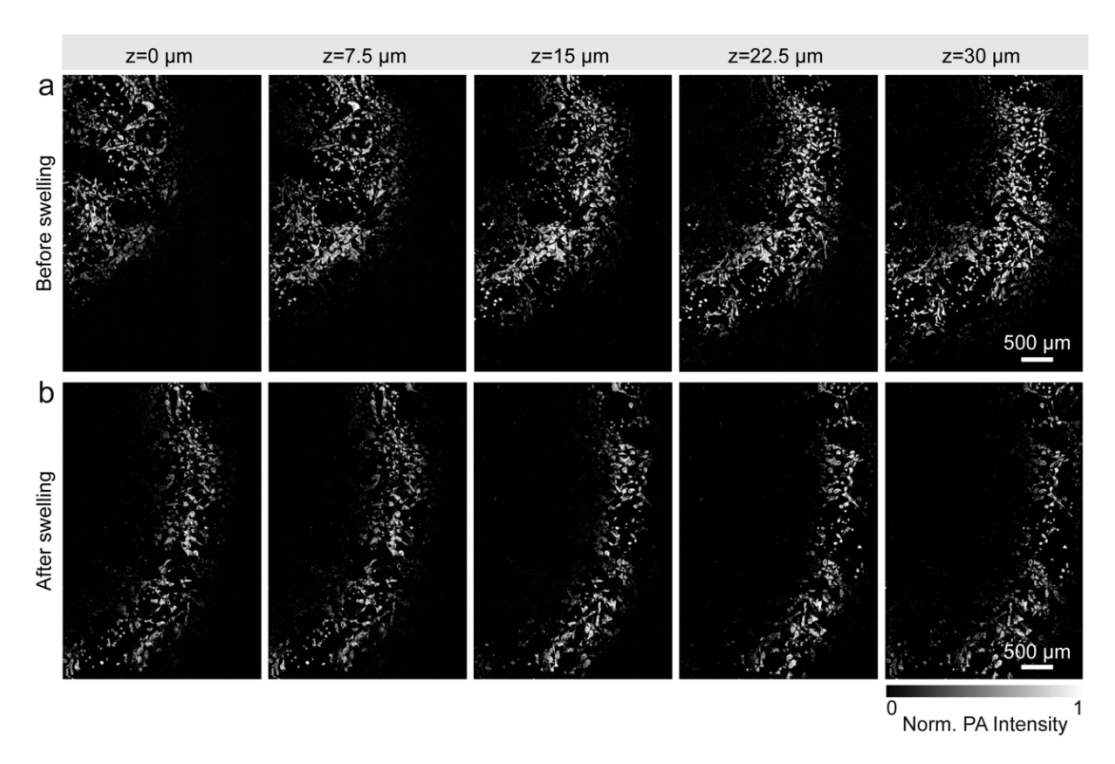


**Fig. S6.** TOR-PAM images of the Vector Blue-stained sample at different depths. (a) Gel before swelling. (b) Gel after swelling in water.

## References

[1] C. Zhang, J.S. Kang, S.M. Asano, R. Gao, E.S. Boyden, Expansion microscopy for beginners: visualizing microtubules in expanded cultured HeLa cells. Curr. Protoc. Neurosci. 92 (2020) e96. <a href="https://currentprotocols.onlinelibrary.wiley.com/doi/full/10.1002/cpns.96">https://currentprotocols.onlinelibrary.wiley.com/doi/full/10.1002/cpns.96</a>.